Physics Open 17 (2023) 100168

Contents lists available at ScienceDirect

Physics Open

journal homepage: www.sciencedirect.com/journal/physics-open

Design and numerical analysis of a novel photonic crystal fiber based chemicals sensor in the THz regime

Md Selim Hossain [a], Rakib Hossen [b], Syada Tasmia Alvi [c], Shuvo Sen [d,*], Md Al-Amin [e], Md. Mahabub Hossain [a]

[a] Department of Electronics and Communication Engineering (ECE), Hajee Mohammad Danesh Science and Technology University (HSTU), Dinajpur, 5200, Bangladesh
[b] Department of Educational Technology (ET), Bangabandhu Sheikh Mujibur Rahman Digital University, Bangladesh Kaliakoir, Gazipur, 1750, Bangladesh
[c] Department of Computer Science and Engineering, Daffodil International University, Dhaka, Bangladesh
[d] Department of Information and Communication Technology (ICT), Mawlana Bhashani Science and Technology University (MBSTU), Santosh, Tangail, 1902, Bangladesh
[e] Department of Electrical and Electronic Engineering (EEE), Daffodil International University (DIU), Dhaka, Bangladesh

ARTICLE INFO

Keywords:
TOPAS-Based PCF
Hexahedron core
EML loss
Larger effective area
High core power fraction
PCF
Scattering loss
Etc

ABSTRACT

We presented a decagonal cladding and hexahedron core-based photonic crystal fiber (PCF) to sense chemicals in the terahertz frequency (THz). Circular air holes (CAHs) in the cladding region make up the proposed sensor. A wide variety of frequencies were evaluated to analyze the sensor's performance in terms of sensitivity, confinement loss, and effective material loss respectively. We designed and quantitatively analyzed the optical properties of our proposed hexahedron-based PCF sensor using the finite element method (FEM). Square-shaped air hole length, strut, and core size have also been researched to improve the performance of the proposed sensor's sensing components and fabrication tolerance. At ideal conditions, the suggested PCF sensor has a maximum relative sensitivity of 94.65%, confinement loss of 6.01×10^{-8} cm^{-1}, effective material loss (EML) of 9.16×10^{-4} cm^{-1}, and effective mode area (EMA) of 1.35×10^{-7} m^2. We are confident that the suggested sensor's optimized geometrical structure will be manufacturing-friendly, as well as the sensor's contribution to practical uses. Furthermore, our proposed PCF fiber will be ideal in the terahertz (THz) regions for various optical communication applications and medicinal signals.

1. Introduction

Detecting an unknown material is a fascinating topic in science, and finding a little particle or analyte anywhere in the world is a required effort. To meet society's needs, researchers are designing and inventing new types of sensors. Some of these compounds are hazardous to human health. Chemicals of the type of ethanol are frequently used for many different things because it is regarded ed a main substance [1]. Alcohol and water are the main analytes because they make up most chemical solutions [2]. Alcohol is colorless and freely flowing, thus many studies have been done on various types of chemical sensing that are connected to alcohol sensing [3,4]. Therefore, a quick and accurate chemical sensing method is needed to ensure the protection of human health. For today's fiber-optic communication, Photonic Crystal Fiber (PCF) is advantageous because it has certain distinct advantages over traditional fiber. Due to this, communication sectors such as telephony, various types of sensing, and so on are boosted [5,6]. The primary method for light to pass through a PCF with the least amount of confinement loss [7], strong nonlinearity [8–10], zero-dispersion [11], and other features is through total internal reflection. The PCFs have advanced to the forefront of liquid and dangerous chemical sensing because of these distinct qualities (guiding light). Along with other optical characteristics, such as effective material loss (EML) [12], birefringence [7], dispersion, confinement loss [13,14], and absorption loss [15], PCF can reduce these by adjusting the air hole diameter or pitch spacing. The qualities listed above are examined for several types of PCF architectures in Refs. [16,17]. [18–20] mentions several outstanding works in chemical sensing. For various analyte types, various PCF sensor types are given in Refs. [21–26]. THz waves usher in a new age in the study of chemical sensing, biomedical engineering, fiber optic communication, and other fields [27,28].

The distance between infrared and microwave rays is covered by this

* Corresponding author.
E-mail address: shuvombstu.it12009@gmail.com (S. Sen).

https://doi.org/10.1016/j.physo.2023.100168
Received 10 May 2023; Received in revised form 11 July 2023; Accepted 17 July 2023
Available online 22 July 2023

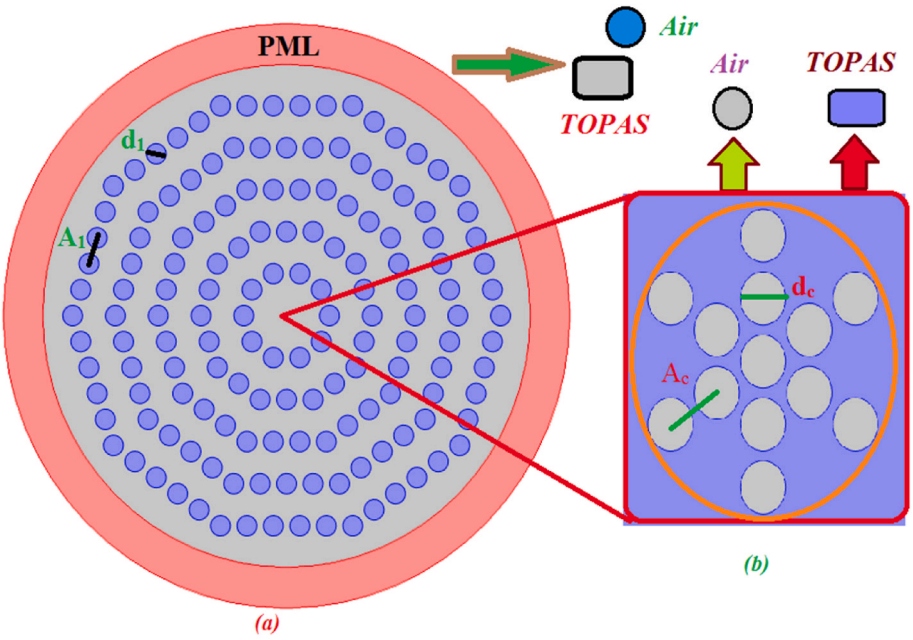

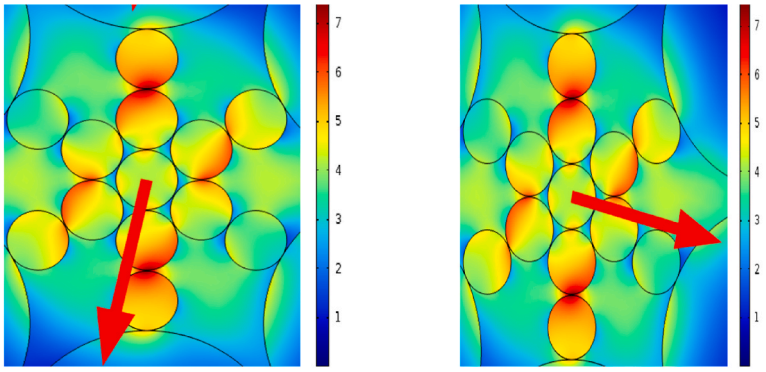

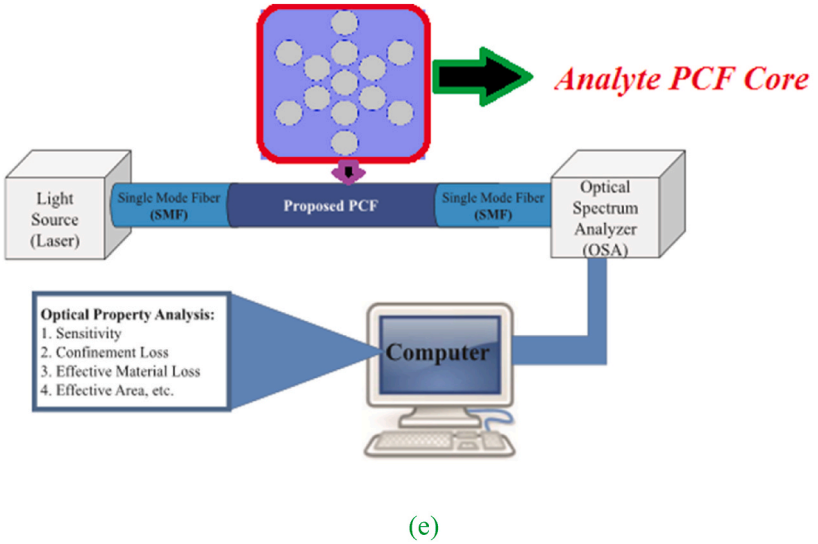

Fig. 1. Designing views of hexahedron-based PCF fiber, (a) decagonal cladding area (b) hexahedron core area. Mode field distributions for (c) polarization of x at the 1 THz. (d) Polarization of y at the 1 THz
Fig. 1(e): Representation of working procedure of the proposed PCF model [5].

region. THz sensing has greater spatial resolution than other sensors and has no ionizing effects, making it more useful than other sensors [29]. In the THz region, several chemical sensing-related research projects have recently been conducted. By presenting a PCF with a folded cladding shape, Paul et al. [21] recently attained a sensitivity of 65.18%. Additionally, in 2017, they used a porous PCF structure to detect alcohol with 69.09% sensitivity [30]. Using TOPAS as a backdrop material, the results were obtained for benzene, ethanol, and water, respectively [31]. Using hexahedron-cored PCF, the authors reported 64% sensitivity for liquid compounds (tabun and sarin liquids) in Ref. [32]. Kanmani et al. in Ref. [33] employed Polytetrafluoroethylene as background material and a slotted core PCF to achieve a sensitivity of 77.08%, 77.18%, and 77.23% for benzene, ethanol, and water, respectively. There are opportunities to increase sensitivity because the findings of all the research do not indicate an acceptable degree of sensitivity.

We presented a Hexahedron PCF in this study to reduce relative sensitivity and simplify fabrication by using a straightforward geometric design for the PCF framework. To find the best structural conditions, which combined high relative sensitivity, low confinement loss, and low effective material loss, we changed the core size and distance between the cladding air holes. The proposed hexahedron PCF sensor features a large core area that will allow a high volume of analyte to be inserted into the core. Additionally, a hollow core fiber's regulated mode is tightly contained within the fiber's core, this significantly minimizes the influence of background material on the wave-guiding characteristics of the fiber [23]. The suggested hexahedron PCF sensor's relative sensitivity and other optical properties have been analyzed using the finite element approach.

2. Design methodology of the single mode PCF

Fig. 1 depicts the geometry of a five-layer air trough (AH) and a two-layer core focus of hexahedron development. The distance is defined by the constraints A_1 and d_1 in the adjourning area which are the accurate arrangement method d_c and A_c are constraints shown in dissimilarity in the rotating core area of the hexahedron. The three chemicals that make up refractive indices are ethanol, benzene, and water. They are centered on their refractive list values (chemicals). Topas, on the other hand, is used to contribute to high RS and high low CL. When the constraints d_1/A_1 are enlarged, they are referred to as the air-filling ratio, which also aids in reducing production problems in the cover zone. Therefore, our PML-based D-PCF and FEM fibers, like RF, CL, AE, total energy factors, and an efficient mode index allow the recovery, from 0.80 tons of terahertz to 3.0 tons of THz, are clearly shown. Here, the PML (boundary condition) of thickness is indicated by the 8% of the maximum fiber diameter and optimized design parameters for core diameter (d_c) = 82 μm, core pitch (Λ_c) = 84 μm, five layers of cladding diameter d1 = d2 = d3 = d4 = d5 = 320 μm and five layers of cladding pitch such as $A_1 = \Lambda_2 = \Lambda_3 = \Lambda_4 = \Lambda_5$ = 380 μm, The PML layer is mainly responsible for confining the structure properly and performing the better to achieve guiding properties such as the relative sensitivity, confinement loss, effective area, and effective mode index according to the terahertz frequency wave range from 0.80 to 3.0 THz.

In Fig. 1(e), light laser is passed through the analytic PCF core, and the optical spectrum analyzer **(OSA)** will provide data to the computer to analyze the optical properties like effective area, RS, CL, and effective mode index of the injected alcohols. Then the computer will represent data numerically and graphically.

3. Results and discussions

To identify the best sensor construction conditions, many parameters were adjusted while considering the relative sensitivity of the suggested hexahedron PCF. Cladding air hole length, structure distance between air holes, and change in core size were the three parameters. By measuring relative sensitivity, the suggested hexahedron PCF's sensing ability was assessed. The following equation was applied to the calculation [18]:

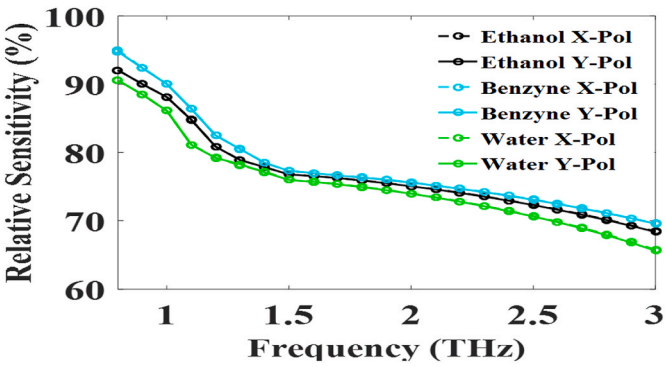

Fig. 2. RS vs 3 chemical frequencies for both polarizations at the ideal conditions.

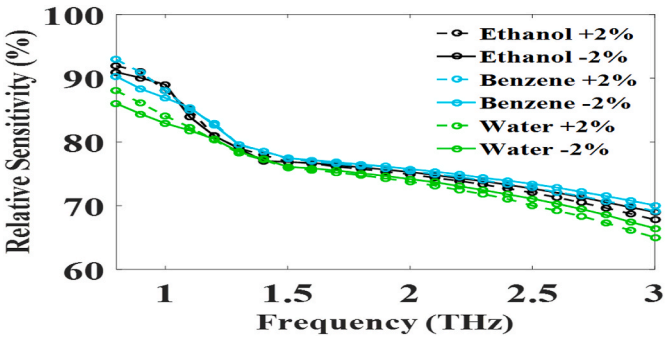

Fig. 3. RS vs 3chemical frequencies for both polarizations at ±2% Variation Parameters.

$$R = \frac{n_a}{n_{eff}} \times P \tag{1}$$

N_a is a representation of the sensing analyte's refractive index. The sensing analyte (n_a) employed in our study has a 1.33 water refractive index. The value of n_{eff}, which indicates the guided mode's effective mode index for the analyte, was acquired from the FEM approach during the simulation regarding various frequencies. The effective mode indices value for the x and y polarization modes is shown in Fig. 2 along with the frequency. The mathematical expression for the power factor ratio, P, is [34]:

$$P = \frac{\left[\int \mathrm{Re}(Ex, Hy, Ey, Hx)\mathrm{dxdy}\right]^1}{\left[\int \mathrm{Re}(Ex, Hy, Ey, Hx)\mathrm{dxdy}^1\right]} x100 \tag{2}$$

Where, Ex and Ey, respectively, stand for the electric fields of the x and y components. Hx and Hy stand for, respectively, the magnetic field in the x- and y-direction.

For equal divergences with perfect parameters and a ±2% change in the parameters, Figs. 2 and 3 are displayed by the RS frequency. From the graphical representation, it can be observed that the RS of ethanol, benzene and water decreases from 1.10 THz to 3 THz due to frequency diversity, and it behaves like an additional accumulative mode from 1.0 THz to 0.8 THz. The numerical data associated with ethanol, benzene, and water, where their respective refractive indices are 1.354, 1.366, and 1.33 and the comparatively sensitive values for them are 92.55%, 94.65%, and 90.30%, respectively.

In PCF fiber, we compute the power fraction by how much power or energy flowing through the PCF structure. Therefore, the power fraction is determined by Ref. [32],

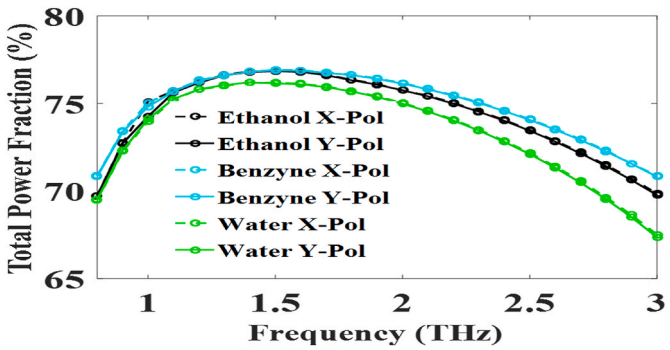

Fig. 4. Total Power fraction vs frequencies are used to determine the best design.

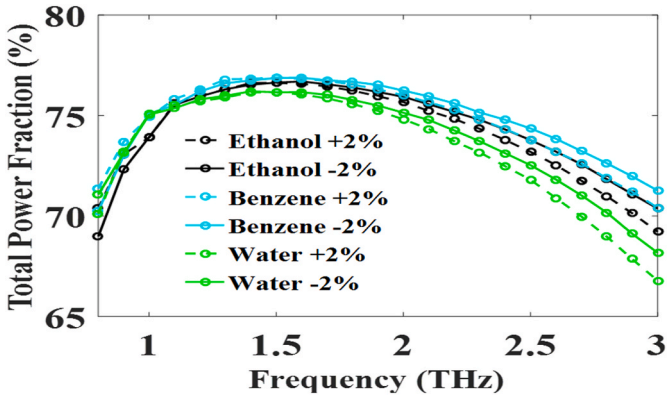

Fig. 5. Total Power percentage vs different frequencies ±2 Variations.

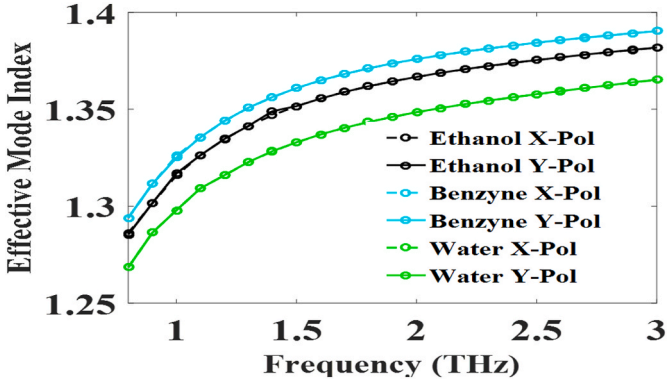

Fig. 6. EMI for both polarizations with respect to the frequencies of 3 substances at the ideal conditions.

$$\eta = \frac{\int_{i} S_z dA}{\int_{all} S_z dA} \tag{3}$$

Here, the nominator integration shows the region of interest such as core, cladding or air hole. Besides, the denominator integration discloses the whole cross-sectional area.

In Fig. 4 shows the power fraction responses with the frequency for both polarizations at the optimal design parameters. Here, it is seen that the power fraction increases according to the frequency range from 0.80 THz to 1.50 THz and then starting decreases the power fraction with the frequency range from 1.60 THz to 3 THz. Here, the power fraction peak values are 79.01, 80.02 and 76.89 for three chemicals such as Ethanol (n = 1.354), Benzene (n = 1.366) and Water (n = 1.330) at 1 THz (THz) frequency.

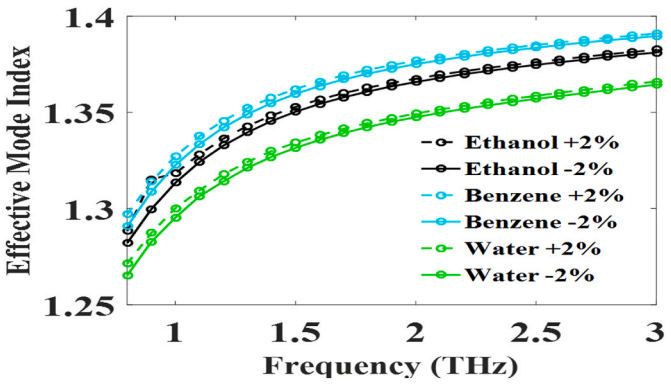

Fig. 7. EMI for ±2% the best possible versions for both polarizations, according to the frequency of 3 substances.

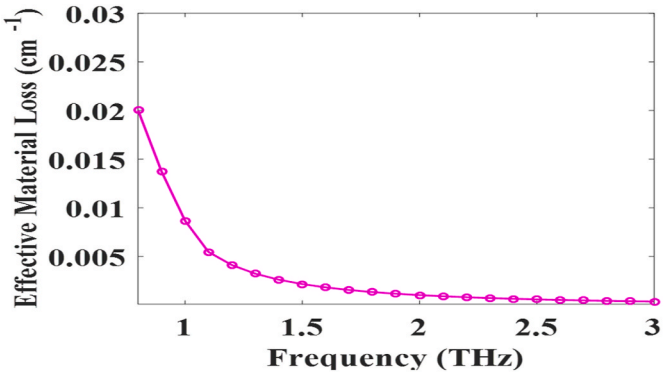

Fig. 8. Effective Mode Index versus functional frequency.

The power fraction responses with the frequency are reported in Fig. 5 for ±2% variations with the optimum design parameters. It is also apparent that the peak value of power fraction is increased with the frequency wave range from 0.80 THz to 1.50 THz and the peak value of power fraction is decreased with the frequency wave pulse from 1.60 THz to 3 THz. Here, 77.60, 78.02 and 77.03 are respectively power fraction peak values for the specified three chemicals such as Ethanol (n = 1.354), Benzene (n = 1.366) and Water (n = 1.330) at 1 THz (THz).

Finally, from Figs. 4 and 5, we find that the peak values are different but the power fraction versus of frequency discloses the similar graphical simulation outputs in the terahertz (THz) wave regions.

Fig. 6 is defined with the effective mode index according to the frequency for x-polarization and y-polarization at the optimum design parameters. We visualize that the effective mode index increases with the frequency is increased. The peak value of the effective mode index value starts at 1.26 with a frequency range of 0.8 THz and the maximum peak value ends at 1.39 according to the maximum frequency range at 3 THz. At 1 THz (THz), 1.29, 1.30, and 1.27 are effective mode index values for three chemicals as Ethanol (n = 1.354), Benzene (n = 1.366), and Water (n = 1.330).

The effective mode index versus the frequency is presented in Fig. 7 for ±2% variations with the optimal design parameters. We also see that the increase of frequency wave ranges with the effective mode index is being increased. Here, the starting peak value of the effective mode index is 1.26 with a frequency range of 0.8 THz and the extreme peak value of the effective mode index is 1.39 according to the frequency range of 3 THz Here, the effective mode index values are 1.31, 1.32 and 1.28 for three chemicals such as Ethanol (n = 1.354), Benzene (n = 1.366) and Water (n = 1.330) at 1 THz (see Fig. 8).

From Figs. 6 and 7, we see clearly that the graphical results of the

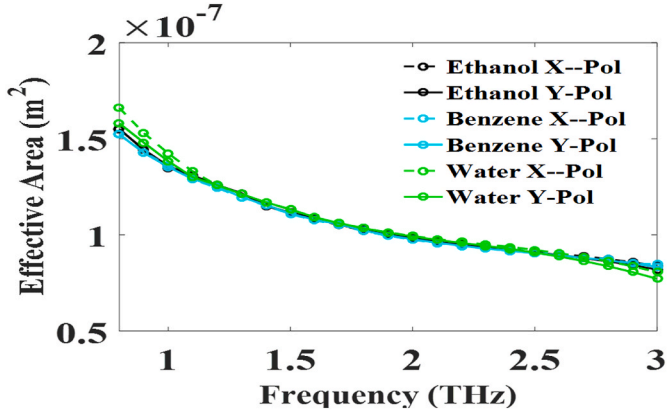

Fig. 9. Effective area region of PCF fiber built at different frequencies.

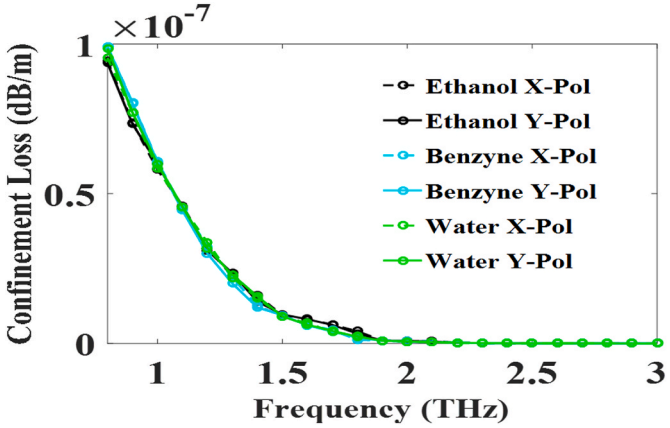

Fig. 10. Optimal design parameters for PCF fiber confinement loss at various frequencies.

effective mode index versus frequency displays a similar output in the terahertz (THz) wave pulse.

The background material of TOPAS creates a very low EML and this EML is calculated by Ref. [32]:

$$\alpha_{ea} = \sqrt{\frac{\varepsilon_0}{\mu_0}} \left(\frac{\int_{mat} n_{mat} |E|^2 \alpha_{mat} \, dAt}{\left| \int_{all} S_{zf} dAt \right|} \right) (\mathrm{cm}^{-1}) \tag{4}$$

In these graphical results, the EML is slightly increased with the frequency and EML is calculated 9.16104 cm.$^{-1}$

We know that the effective area is the most essential optical property in any PCF fiber. Moreover, the larger effective area based PCF sensor shows the high relative sensitivity and the low confinement loss. Here, the effective area is defined by Ref. [31],

$$A_{eff} = \frac{\left[\int I(rt) rtdrt \right]^2}{\left[\int I^2(rt) drt \right]^2}, \mathrm{m}^2 \tag{5}$$

Where, the effective area is A_{eff} and the cross sectional electric field intensity is $I(r) = |A_{ff}|^2$.

In Fig. 9 shows the effective area according to the frequency of the reported D-PCF fiber for optimum design parameters. Here, the effective area decreases with the increases frequency range from 0.8 THz to 3 THz. In addition, the large effective area displays the high relative sensitivity and the low confinement loss in the terahertz (THz) waveguide. At operating region of 1 THz, the effective area for water, benzene and ethanol are 1.44×10^{-7}, 1.35×10^{-7} m^2 and 1.34×10^{-7} m^2.

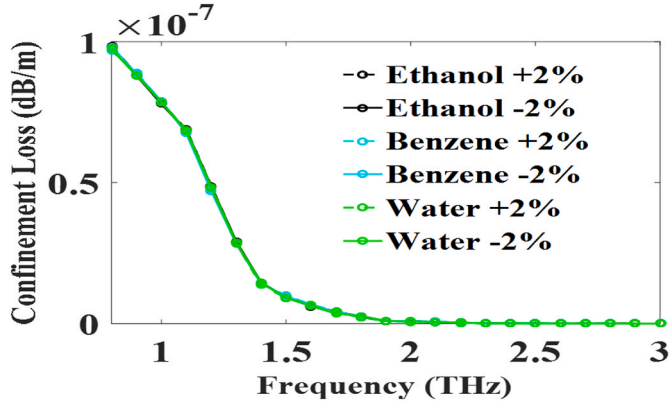

Fig. 11. The suggested PCF fiber's confinement loss at various frequencies with ±2 Variations.

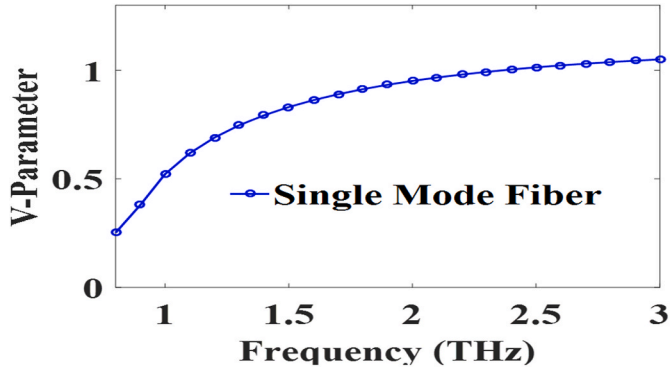

Fig. 12. For the best design, different frequencies are used to compute the V-parameter of the developed SM-PCF.

Confinement loss is another important optical characteristic in the PCF structure. Moreover, the low confinement loss PCF fiber displays the high relative sensitivity. Thus, confinement or leakage loss L_c is defined by Ref. [30],

$$L_c = 8.686 \times K_0 \, \mathrm{Im} \left[n_{eff} \right] \ (\mathrm{dB} / \mathrm{m}) \tag{6}$$

Here, $K_0 = 2\pi \left(\frac{f}{c} \right)$, the speed of photon is c and the frequency is f. Besides, the effective mode index as an imaginary part is I_m (n_{eff}).

In Fig. 10 discloses the confinement loss responses with frequency in the optimal design parameters. We see that the confinement loss decreases according to the increasing of frequency wave pulse. We also see that the confinement losses stay flat according to the frequency range from 2.10 THz to 3 THz. The confinement losses are 5.81×10^{-08}, 5.75×10^{-08} dB/m 6.01×10^{-08} dB/m and 5.84×10^{-08} dB/m for chemicals such as Ethanol (n = 1.354), Water (n = 1.330) and Benzene (n = 1.366) at 1 THz.

In Fig. 11 displays the confinement loss according to the frequency for variations ±2% with the optimum design parameters. Here, we also see from this figure that the confinement loss is decreased with the increasing of frequency. In addition, the confinement losses also remain constant according to the frequency range from 2.10 THz to 3 THz. Here, 7.81×10^{-08}, 7.83×10^{-08} dB/m and 7.88×10^{-08} dB/m are confinement losses for three chemicals such as Ethanol (n = 1.354), Benzene (n = 1.366) and Water (n = 1.330). After investigating Figs. 10 and 11, we see that the confinement loss versus of frequency shows the similar graphical results.

V-parameter displays the single mood communication, and the V-parameter is shown the following equation [29]:

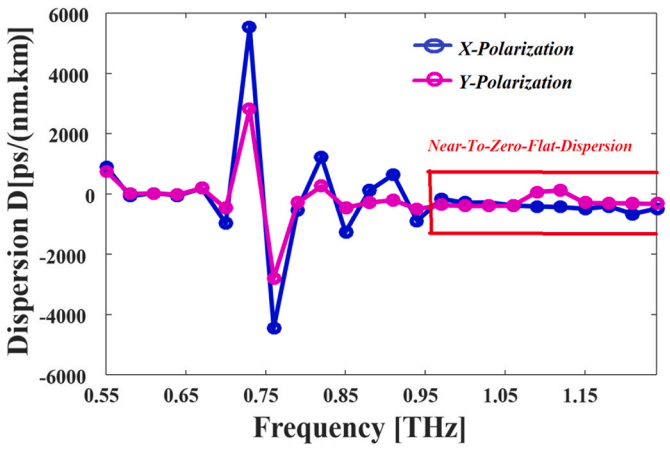

Fig. 13. Dispersion curve as a function of the ideal PCF structure's frequency.

Table 1
The table displays the best values around 1 THz with ±2% variations.

Parameters (%)	Relative sensitivity (%)			Confinement loss (dB/m)		
	Ethanol	Benzene	Water	Ethanol	Benzene	Water
+2%	93.20	95.52	91.24	7.81×10^{-08}	7.88×10^{-08}	7.83×10^{-08}
Optimum	92.55	94.65	90.30	5.80×10^{-08}	6.01×10^{-08}	5.75×10^{-08}
−2%	91.04	93.34	88.95	7.31×10^{-08}	7.58×10^{-08}	7.70×10^{-08}

$$V = \frac{2\pi ef}{c}\sqrt{ne_{coe}^2 - ne_{cle}^2} \leq 2.045 \quad (7)$$

Where, the core and cladding area based effective mood index is defined by the n_{coe} and n_{cle} and c is the radius of the core.

In this graphical Fig. 12, the V-parameter is increasing with the frequency ranges from 0.80 to 3 THz and this V-parameter shows single mood communication system (V −parameter ≤ 2.045) (see Fig. 13).

Dispersion in optical fiber refers to the spreading or broadening of optical signals as they propagate through the fiber. This phenomenon arises due to the different propagation speeds of different wavelengths of light, causing the pulses to spread out over distance and time. The dispersion profile is directly impacted by the PCF's ERI. The value of β, which is modality propagation constant, is derivable by means of the Taylor expansion in second order, as illustrated in Ref. [24]:

$$\beta_2 = \frac{2}{c}\frac{dn_{eff}}{d\omega} + \frac{\omega}{c}\frac{d^2n_{eff}}{d\omega^2}, [\text{ps / THz / cm}] \quad (8)$$

The propagation mode has two polarizations (x and y polarizations), $N_{eff} = \text{Re}(\beta)\omega/c$ and $\omega = 2\pi f$. The two polarizations that are utilized in the x and y propagation modes. In Fig. 12, it showed how to apply equations. The close-fitting behavior of polarization curves on both exerting left and right, they turned themselves is nicely shown in Fig. 12. In a wider frequency band, an even distribution between 0.97 THz and 1.09 THz that is nearly nil has been observed.

Sometimes, it is feasible to simultaneously transmit several optical signals with similar pulse spreads. The transmitted optical signal's bandwidth can be increased thanks to the lower dispersion value. A flattened dispersion around zero is also seen over a more comprehensive frequency range of 0.97 THz to 1.09 THz. On certain occasions, it is possible for multiple optical signals to be transmitted at the same time, with their pulse spread being almost identical. The transmitted optical signal's bandwidth can be increased thanks to the lower dispersion value. The proposed fiber exhibits this behavior with optical parameters, which is advantageous.

The optimal design and designs for optical options like the RS and CL of the PCF have both demonstrated contrasts of around ±2%. Table 1 demonstrates the ±2% variations' modest sum of significant differences, and the RS and CL are best for unwinding. Thus, to avoid the manufacturer's intricacy, we use superior plans. We are therefore prepared to state unequivocally that the suggested PCF, configuration is considered more suitable for industrial or biomedical applications, considering the positioning of the chemicals is involved.

Finally, Table 2 demonstrates that the recommended optical sensor based on decagonal spectroscopy has a greater PCF than the other PCFs. As a result, when the PCF is placed, it will be crucial in optical waveguides as well as optical devices.

Here, D-PCF framework's innovative approach is a crucial element. The most popular construction techniques, including passenger plug, sol-gel, tiresome, attraction, and stack, are currently used to create PCFs. Recently, the method of Sol-gel [32,33] has been investigated as a means of improving sensor PCFs. However, this specific filling technique [42, 43] leads to the center zones' filling of chemicals or in any stack containing PCF fibers. Superior management characteristics like RS, accidents, EA, TPF, and EMI are improved because of choosing the feasible investigation on this particular supplemental method.

4. Conclusion

We proposed a decagonal cladding and a photonic crystal fiber core based on hexahedron (PCF) for sensory chemical applications. The THz frequency region proposed to sensitize chemicals by decagonal cladding air lights and hexahedron shaped core structure-oriented Hexahedron PCF. The relative sensitivity of 94.65% improved by changing the hexahedron core's proposed geometrical design of the PCF at 1 THz operating frequency. In addition, a loss in confinement of 6.01×10^{-8} cm^{-1} was obtained at ideal circumstances for the suggested PCF sensor, an effective material loss of 9.16×10^{-4} cm^{-1} and an efficient mode area of 1.35×10^{-7} m^2 has been gathered under ideal circumstances for the suggested PCF sensor. We are confident that the proposed sensor's improved geometrical structure will make it easy to fabricate and that it will be useful in practical applications.

Table 2
The comparison table compares the optical characteristics of the decagonal PCF structure to those of other PCFs.

Prior in PCFs	Operating region	Relative Sensitivity (%)	Confinement loss (dB/m)	Design of structure	
				Core	Cladding
PCF_1 [35]	f = 1 THz	60.05	1.43×10^{-11}	Rotated-Hexa circular holes	Heptagonal
PCF_1 [36]	f = 1.2 THz	64.00	1.12×10^{-11}	Elliptical holes	Quasi
PCF_1 [37]	f = 1 THz	74.54	7.72×10^{-08}	slotted core	Quasi
PCF_1 [38]	f = 1.3 THz	78.80	2.19×10^{-09}	Elliptical holes	Quasi
PCF_1 [39]	f = 1 THz	45.13	5.583×10^{-05}	Circular holes	Hexagonal
PCF_1 [40]	f = 1 THz	55.56	1.00×10^{-05}	Rhombic holes	Hexagonal
PCF_1 [41]	f = 1 THz	80.93	1.23×10^{-11}	Elliptical hole	Circular
Proposed D-PCF	f = 1 THz	94.65	6.01×10^{-08}	Hexahedron	Decagonal

Declaration of competing interest

The authors declare that they have no conflict of interest.

Data availability

The data that has been used is confidential.

Acknowledgement

The authors do not receive any funding for this research work.

References

[1] K. Wang, Metal wires for terahertz wave guiding, Nature 432 (2004) 376–379.
[2] E.R. Vera, J.U. Restrepo, C.J. Durango, J.M. Cardona, N.G. Cardona, Design of low loss and highly birefringent porous core photonic crystal fiber and its application to terahertz polarization beam splitter, IEEE Photon. J. 10 (4) (2018).
[3] L. Ho, M. Pepper, P. Taday, Terahertz spectroscopy: signatures and fingerprints, Nat. Photonics 2 (9) (2008) 541.
[4] S. Rana, A.S. Rakin, M.R. Hasan, M.S. Reza, R. Leonhardt, Low loss and flat dispersion kagome photonic crystal fiber in the terahertz regime, Opt Commun. 410 (2018) 452–456.
[5] M.S. Hossain, S. Shuvo, M.M. Hossain, Design of a chemical sensing circular photonic crystal fiber with high relative sensitivity and low confinement loss for terahertz (THz) regime, Optik - International Journal for Light and Electron Optics 222 (2020), 165359, https://doi.org/10.1016/j.ijleo.2020.165359 (2020).
[6] Jianying Zhou, Yu Zheng, Fiber refractive index sensor with lateral-offset micro-hole fabricated by femtosecond laser, Optik 185 (2019) 1–7, https://doi.org/10.1016/j.ijleo.2019.03.094(2019). ISSN 0030-4026.
[7] N.R. Ramanujam, KS Joseph Wilson, P. Mahalakshmi, Sofyan A. Taya, Analysis of photonic band gap in photonic crystal with epsilon negative and double negative materials, Optik 183 (2019) 203–210, https://doi.org/10.1016/j.ijleo.2019.02.066. ISSN 0030-4026.
[8] Y.S. Jin, G.J. Kim, S.G. Jeon, Terahertz dielectric properties of polymers, J. Kor. Phys. Soc. 49 (2) (2006) 513–517.
[9] H. Ilatikhameneh, T. Ameen, F. Chen, H. Sahasrabudhe, G. Klimeck, R. Rahman, Dramatic impact of dimensionality on the electrostatics of P-N junctions and its sensing and switching applications, IEEE Trans. Nanotechnol. (2018), https://doi.org/10.1109/TNANO.2018.2799960.
[10] L.J. Chen, H.W. Chen, T.F. Kao, J.Y. Lu, C.K. Sun, Low-loss subwavelength plastic fiber for terahertz waveguiding, Opt Lett. 31 (3) (2006) 308–310.
[11] J.Y. Lu, C.P. Yu, H.C. Chang, H.W. Chen, Y.T. Li, C.L. Pan, C.K. Sun, Terahertz air-core microstructure fiber, Appl. Phys. Lett. 92 (6) (2008), 064105.
[12] T. Ritari, J. Tuominen, H. Ludvigsen, J.C. Petersen, T. Sorensen, T.P. Hansen, H. R. Simonsen, Gas Sensing Using Air-Guiding Photonic Bandgap Fibers, Opt. Express, 2004, pp. 4080–4087.
[13] H. Ademgil, S. Haxha, F. AbdelMalek, Highly nonlinear bending-insensitive birefringent photonic crystal fibres, Engineering 2 (8) (2010) 608.
[14] J.H. Lee, P.C. Teh, Z. Yusoff, M. Ibsen, W. Belardi, T.M. Monro, D.J. Richardson, A holey fiber-based nonlinear thresholding device for optical CDMA receiver performance enhancement, IEEE Photon. Technol. Lett. 14 (6) (2002) 876–878.
[15] D. Devi, Structural parameters, electronic properties, and band gaps of a single walled carbon nanotube: a pz orbital tight binding study, Superlattice. Microst. (2018), https://doi.org/10.1016/j.spmi.2018.05.023.
[16] S. Shuvo, M.A. Shafi, A.S. Sikder, MdS. Hossain, M.M. Azad, Zeonex based decagonal photonic crystal fiber (D-PCF) in the terahertz (THz) band for chemical sensing applications, Sens. Bio-Sens. Res. (2020), https://doi.org/10.1016/j.sbsr.2020.100393.
[17] M.S. Hossain, S. Sen, Design and Performance Improvement of Optical Chemical Sensor Based Photonic Crystal Fiber (PCF) in the Terahertz (THz) Wave Propagation. Silicon, 2020, https://doi.org/10.1007/s12633-020-00696-8.
[18] M.S. Islam, J. Sultana, M. Dorraki, J. Atai, M.R. Islam, A. Dinovitser, D. Abbott, Low loss and low dispersion hybrid core photonic crystal fiber for terahertz propagation, Photonic Netw. Commun. 35 (3) (2018) 364–373.
[19] S.F. Kaijage, Z. Ouyang, X. Jin, Porous-core photonic crystal fiber for low loss terahertz wave guiding, IEEE Photon. Technol. Lett. 25 (15) (2013) 1454–1457.
[20] K. Ahmen, B.K. Paul, S. Chowdhury, S. Sen, M.I. Islam, M.S. Islam, Design of a single mode photonic Crystal fiber with ultra-low material loss and large effective mode area in THz regime, IET Optoelectron. 11 (6) (2017) 265–271.
[21] G.K.M. Hasanuzzaman, M.S. Habib, S.A. Razzak, M.A. Hossain, Y. Namihira, Low loss single-mode porous-core kagome photonic crystal fiber for THz wave guidance, J. Lightwave Technol. 33 (19) (2015) 4027–4031.
[22] M.M. Rahman, F.A. Mou, M.I.H. Bhuiyan, M.R. Islam, Extremely Low Effective Material Loss of Air Core Photonic Crystal Fiber for THz Guidance, IEEE Region 10 Symposium (TENSYMP), Kolkata, India, 2019, pp. 716–720, https://doi.org/10.1109/TENSYMP46218.2019.8971297(2019).
[23] R.K. Gangwar, V.K. Singh, Study of highly birefringence dispersion shifted photonic crystal fiber with asymmetrical cladding, Optics 127 (24) (2016) 11854–11859.
[24] M.R. Hasan, S. Akter, T. Khatun, A.A. Rifat, M.S. Anower, Dual-hole unit-based kagome lattice microstructure fiber for low-loss and highly birefringent terahertz guidance, Opt. Eng. 56 (4) (2017), 043108.
[25] Y.S. Lee, C.G. Lee, Y. Jung, M.K. Oh, S. Kim, Highly Birefringent and dispersion compensating photonic crystal fiber based on double line defect core, J. Opt. Soc. Korea 20 (5) (2016) 567–574.
[26] M.M. Hasan, M. Barid, M.S. Hossain, et al., Large effective area with high power fraction in the core region and extremely low effective material loss-based photonic crystal fiber (PCF) in the terahertz (THz) wave pulse for different types of communication sectors, J. Opt. 50 (2021) 681–688, https://doi.org/10.1007/s12596-021-00740-9.
[27] R. Islam, S. Rana, R. Ahmad, S.F. Kaijage, Bend-Insensitive and low-loss porous core spiral terahertz fiber, IEEE Photon. Technol. Lett. 27 (21) (2015) 2242–2245, https://doi.org/10.1109/LPT.2015.2457941.
[28] M.R. Hasan, M.A. Islam, M.S. Anower, S.M.A. Razzak, Low-loss and bend-insensitive terahertz fiber using a rhombic-shaped core, Appl. Opt. 55 (2016) 8441–8447.
[29] M.M. Awad, R.A. Cheville, Transmission terahertz waveguide based imaging below the diffraction limit, Appl. Phys. Lett. 86 (22) (2005), https://doi.org/10.1063/1.1942637, 221107221107-3.
[30] S. Rana, A.S. Rakin, M.R. Hasan, M.S. Reza, R. Leonhardt, D. Abbott, H. Subbaraman, Low loss and flat dispersion Kagome photonic crystal fiber in the terahertz regime, Opt Commun. 410 (2018) 452–456.
[31] J. Sultana, M.S. Islam, M. Faisal, M.R. Islam, B.W.H. Ng, H. Ebendorf-Heidepriem, D. Abbott, Highly birefringent elliptical core photonic crystal fber for terahertz application, Opt Commun. 407 (2018) 92–96.
[32] Md Abdullah-Al-Shafi, Nasima Akter, Shuvo Sen, Md Selim Hossain, Design and performance analysis of background material of zeonex based high core power fraction and extremely low effective material loss of photonic crystal fiber in the terahertz (THz) wave pulse for many types of communication areas, Optik 243 (2021), 167519, https://doi.org/10.1016/j.ijleo.2021.167519. ISSN 0030-4026.
[33] F.A. Mou, M.M. Rahman, A.A. Mahmud, M.I.H. Bhuiyan, M.R. Islam, Design and Characterization of a Low Loss Polarization Maintaining Photonic Crystal Fiber for THz Regime, IEEE International Conference on Telecommunications and Photonics, 2019.
[34] K. Ahmed, S. Chowdhury, B.K. Paul, M.S. Islam, S. Sen, M.I. Islam, et al., Ultrahigh birefringence, ultralow material loss porous core single-mode fiber for terahertz wave guidance, Appl. Opt. 56 (12) (2017) 3477–3483, https://doi.org/10.1364/AO.56.003477.
[35] M.R. Hasan, M.A. Islam, A.A. Rifat, A single mode porous-core square lattice photonic crystal fiber for THz wave propagation, J. Eur. Opt. Soc. Rapid. Publ. 12 (1) (2016) 15, https://doi.org/10.1186/s41476-016-0017-5.
[36] K. Ahmed, S. Chowdhury, B.K. Paul, M.S. Islam, S. Sen, M.I. Islam, Ultrahigh birefringence, ultralow material loss porous core single-mode fiber for terahertz wave guidance, Appl. Opt. 56 (12) (2017) 3477–3483, https://doi.org/10.1364/AO.56.003477.
[37] S. Rana, G.K. Hasanuzzaman, S. Habib, S.F. Kaijage, R. Islam, Proposal for a low loss porous core octagonal photonic crystal fiber for T-ray wave guiding, Opt. Eng. 53 (11) (2014), https://doi.org/10.1117/1.OE.53.11.115107, 115107–115107.
[38] Md Saiful Islam, J. Sultana, K. Ahmed, M. Rakibul Islam, A. Dinovitser, B. Wai-Him Ng, D. Abbott, A novel approach for spectroscopic chemical identification using photonic crystal fiber in the terahertz regime, IEEE Sensor. J. 18 (2018) 575–582.
[39] Md Saiful Islam, J. Sultana, A.A. Rifat, A. Dinovitser, B. Wai-Him Ng, D. Abbott, Terahertz sensing in a hollow core photonic crystal fiber, IEEE Sensor. J. 18 (2018) 4073–4408.
[40] M.R. Hasan, M.A. Islam, M.S. Anower, S.M. Razzak, Low-loss and bend-insensitive terahertz fiber using a rhombic-shaped core, Appl. Opt. 55 (30) (2016) 8441–8447, https://doi.org/10.1364/AO.55.008441.
[41] G.K.M. Hasanuzzaman, S. Rana, M.S. Habib, A novel low loss, highly birefringent photonic crystal Fiber in THz regime, IEEE Photon. Technol. Lett. 28 (April 8) (2016) 899–902.
[42] F.A. Mou, M.M. Rahman, M.R. Islam, M.I.H. Bhuiyan, Development of a photonic crystal fiber for THz wave guidance and environmental pollutants detection, Sens. Bio-Sens. Res. 29 (100346) (2020).
[43] R. Islam, S. Rana, R. Ahmad, S.F. Kaijage, Bend-insensitive and low-loss porous core spiral terahertz fiber, IEEE Photon. Technol. Lett. 27 (21) (2015) 2242–2245, https://doi.org/10.1109/LPT.2015.2457941.